CI&CEQ
Chemical Industry & Chemical Engineering Quarterly

Available online at
Association of the Chemical Engineers of Serbia AChE
www.ache.org.rs/CICEQ

Chem. Ind. Chem. Eng. Q. 29 (4) 281–289 (2023) CI&CEQ

SEVGI CAN GÖL
ELIF AKBAY

Eskişehir Technical University, Dept. of Chemical Engineering, İki Eylül Campus, Eskişehir, Turkey

THE EFFECT OF METAL-TITANIA INTERACTION ON PHOTODEGRADATION IN SBA-15-SUPPORTED METAL-TITANIA PHOTOCATALYSTS

Article Highlights

- Several transition metals were inserted into the Ti-SBA-15 by using two-step synthesis methods
- Co-Ti-SBA-15 is a suitable photocatalyst with the highest photocatalytic activity for dye
- The enhanced activity comes from the increased electron transfer mobility due to metal doping
- Co-Ti-SBA-15 has high stability in dye degradation over five-run without any structural deviation

Abstract

Several transition metals (Fe, Cu, Ni, Cr, and Co) were inserted into the Ti-SBA-15 using two-step synthesis methods. XRD, SEM-EDX, N_2 adsorption-desorption isotherms, XRF, and UV-DRS analysis were used for characterizations. The results confirmed preserving an ordered mesoporous structure, well-dispersed Ti-metal and enhanced light absorption compared with Ti-SBA-15. The photocatalytic performances were evaluated in the degradation of methylene blue under UV light. The results show that the Co-Ti-SBA-15 exhibited the highest photocatalytic activity among the prepared photocatalysts for the degradation of methylene blue. The significant activity increase might be attributed to the increased reactant adsorption by the mesoporous structure of SBA-15, the good distribution of TiO_2 in the pores of SBA-15, and the increased electron transfer mobility due to metal doping. In addition to efficiency, Co-Ti-SBA-15 is a suitable catalyst for dye degradation, exhibiting good stability in methylene blue degradation over five photocatalytic runs without any deviation of the structure.

Keywords: transition metals, mesoporous material, Ti-SBA-15, photocatalytic degradation, reusability.

SCIENTIFIC PAPER

UDC 544.526.5:546:66

Photocatalysis is mainly used for the abetment of environmental pollutants and has been attractive to researchers worldwide [1]. Photocatalysis can be superior to other widely used methods, such as oxidation, absorption, ion exchange, etc. [2]. Some semiconductors (TiO_2, Fe_2O_3, ZnO, ZrO_2, Nb_2O_5, SnO_2, and others) and a number of nanocomposites such as Ag-Mn_xO_y, WO_3/g-C_3N_4, g-C_3N_4/ $CdWO_3$, and TiO_2-SnO_2-Sb_2O_5-NiO-carbon nanotubes have been used as photocatalysts and have attracted significant attention due to their wide application for pollution abetment [3–8].

Most importantly, TiO_2 is widely used because of its high photo-stability, low toxicity, commercial availability, and large band gap of 3.2 eV [9–11]. However, its photocatalytic activity is restricted by specific parameters such as low surface area, coagulation in aqueous media, and separation and recycling problems [12]. This limitation may be overcome when dispersed on mesoporous silica support such as Santa Barbara Amorphous (SBA-15).

Correspondence: E. Akbay, Eskişehir Technical University, Dept. of Chemical Engineering, İki Eylül Campus, Eskişehir, 26555, Turkey.
E-mail: eodes@eskisehir.edu.tr
Paper received: 17 October, 2022
Paper revised: 27 December, 2022
Paper accepted: 10 January, 2023

https://doi.org/10.2298/CICEQ221017001G

SBA-15 is a significant mesoporous silica noted for its high surface area, narrow pore size distribution, uniform meso porosity, low cost, and biodegradable template [2,13]. Immobilization of TiO_2 into the SBA-15 could reduce the particle size of TiO_2 and thereby avoid aggregation. The synthesized material is a more effective photocatalyst than commercial Degussa P25 or another synthesized nanoparticle form. There are many studies on different synthesizing methods and optimum TiO_2 loading to synthesize Ti-SBA-15 in the literature [14–17]. The Si/Ti ratio is critical at approximately sixteen because its low or high values defect the mesopore structure of SBA-15 and decrease photocatalytic efficiency [16–18].

TiO_2-SBA-15 can be useful for photocatalysis but can absorb only 4% of the spectrum [19]. On the other hand, doping TiO_2-SBA-15 by metals such as Ag [20], Au [21], W [22], Fe [19], CoMo [23], Sn [24], and Pt [25] extends the response to a wide range of the spectrum and exhibits a synergistic effect on narrowing of the TiO_2 band gap up to 1.45 eV [4]. In these papers, titanium was successfully inserted into the SBA-15 structure by different methods using organic titanium sources and then metal doping by post-synthesized methods. The obtained nanocomposites enhanced the reactant adsorption by the mesoporous structure of SBA-15 with a good distribution of TiO_2, as well as reduced electron-hole recombination rates due to metal doping. As a result, a significant enhancement in photocatalytic activity under visible light or UV has been obtained for the degradation of organic pollutants and the production of added-value chemicals.

Therefore, in this paper, the Ti-SBA-15 composite was prepared by the direct synthesized method using a TiO_2 nano-powder source. To enhance the extended range of the spectrum of TiO_2, a number of transition metal nanoparticles (Cu, Fe, Co, Cr, and Ni) were chosen for doping on the surface of the TiO_2/SBA-15 because transition metals have good electron changeability enhancing catalytic activity, anti-poisoning property, longevity, regeneration, and low cost [26]. The composition, morphology, and optical properties of synthesized photocatalysts are characterized by XRD, SEM-EDX, XRF, UV-DRS, and N_2 adsorption-desorption isotherms. In addition, the photocatalytic activity and stability of the photocatalysts have been evaluated for the degradation of methylene blue under UV light irradiation. Finally, the reused photocatalysts have been tested to determine any structural deviation using XRD, SEM-EDX, and N_2 adsorption-desorption isotherms.

MATERIALS AND METHODS

Chemicals

The tetraethyl orthosilicate (TEOS), Pluronic-123 ((triblock poly(ethylene oxide)-poly(propylene oxide)-poly(ethylene oxide) were bought from Sigma Aldrich. The HCl (37%) was obtained from Riedel-de Haen. The TiO_2 nano-powder, Degussa-P25, and methylene blue were obtained from Merck. The iron (III) nitrate nonahydrate (Fe $(NO_3)_3$. $9H_2O$), Copper (II) nitrate trihydrate (Cu $(NO_3)_2.3H_2O$), Chromium (III) nitrate nonahydrate (Cr $(NO_3)_3.9H_2O$), and Cobalt (II) nitrate hexahydrate (Co $(NO_3)_2.6H_2O$) were supplied by Carlo Erba Reagents. The nickel (II) nitrate hexahydrate (Ni $(NO_3)_2.6H_2O$) was bought from Roth.

Synthesis

The SBA-15 synthesis procedure was given in previous work [27]. The addition of TiO_2 modified this method; 4 g of Pluronic-123 was added to 30 mL of distilled water in a magnetic stirrer at 35 °C for 3 h, after which 150 mL of 2 M HCl was added. In this step, the amount of nano-TiO_2 adjusted to Si/Ti=16 was added to the solution and mixed for two hours, then 9 mL of TEOS was added. The obtained mixture was stirred for twenty hours at 40 °C and was aging to react at 100 °C overnight in Teflon. The samples were filtered and washed with deionized water to remove excess HCl. Drying was carried out at 30 °C for forty-five hours, and calcination was applied at 600 °C under airflow for five and a half hours.

In the metal doping step; 1 g of TiO_2/SBA-15 was dispersed in 10 mL of an aqueous solution of $Fe(NO_3)_3$, $Cr(NO_3)_3$, $Ni(NO_3)_2$, and $Cu(NO_3)_2$ at a loading amount of 10 wt.% by an ultrasonic homogenizer for 15 min. The resulting solution was dried in an oven at 110 °C. Next, the dried sample was calcined at 300 °C for two hours at a heating rate of 5 °C/min. Finally, the sample was washed three times with 250 mL distilled water and dried in an oven at 80 °C for twelve hours.

Characterization

X-ray diffraction (XRD) analyses were performed by an X-ray diffractometer (RigakuRind XRD MiniFlex 300/600) and Cu-Kα (1.54 Aº) radiation (40kV-15mA) with scanning from 2Θ=70° to 2Θ=5° at a rate of 2° per minute^{-1}. The crystallite sizes of the samples were found using Scherrer's equation of $D=k\lambda/\beta\cos\theta$ where D is the crystallite diameter, λ is the radiation wavelength (1.5406Å), β is the peak full with half maximum (FWHM), θ is the diffracting angle and k=0.90 for the spherical shape particle.

Surface analysis of the photocatalysts was performed by a HITACHI TM 3030 Plus branded SEM device. XRF analysis was carried out by Rigaku ZSX Primus II. The BET (Brunauer-Emmett-Taller) specific surface area was calculated from N_2 adsorption-desorption isotherms measured at 77 K in an automatic

adsorption apparatus (Tristar II 3020 Operator Manual v3.02, Micrometric). Degassing of the samples was at 250 °C for four hours. The pore size distributions of the catalysts were given using the Barrett-Joyner-Halenda (BJH) method. UV Diffuse Reflectance Spectra (DRS) were achieved from 200 to 700 nm using a UV-vis spectrophotometer (Shimadzu UV-3600).

Photocatalytic reactions

Photocatalytic degradation of methylene blue was performed in a quartz reactor system equipment with a temperature controller. The reactor system had a thin layer of aluminum foil with 99 % purity. The light source was four 8 W UV (364 nm) low-pressure mercury lamps.

In a typical experiment, 20 mg/L of 150 mL methylene blue at natural pH was taken, and 75 mg of the catalyst was added to the solution. The reaction mixture was magnetically stirred for one hour to reach the adsorption-desorption equilibrium without light. Then, taking 2 mL of the solution, the catalyst was taken by centrifugation at 13000 rpm for twenty minutes. The concentration of the samples was measured by Spectrophotometer (SHIMADZU UV-2600 UV) at 664 nm. The conversion of methylene blue was calculated by dividing the concentration of methylene blue consumed during the reaction by its initial concentrations. After the photocatalytic reaction, the catalyst was collected from the reaction solution by centrifugation and reused five times. Before the following cycle, the catalyst was washed with ethanol and dried on filter paper to separate the methylene blue in the photocatalyst.

RESULTS AND DISCUSSION

To examine the structural properties of M-Ti-SBA-15, XRD, SEM-EDX, XRF, UV-DRS, and N_2 adsorption-desorption isotherms analyses were carried out after the metal doping. In addition, the photocatalytic activity of M-Ti-SBA-15 was evaluated on the degradation of methylene blue.

Morphological, textural, and optical properties of M-Ti-SBA-15

The photocatalysts were examined using low-wide angle XRD patterns given in Figures 1a and 1b. As can be seen in Figure 1a, the XRD patterns show a reflection peak at $2\Theta \cong 0.8°$, which is evidence that it had maintained the 2D hexagonal meso structure of SBA-15 in the synthesized catalysts [19,28]. However, the insertion of the metal decreases the peak intensities. As a result, it creates a tiny contradiction of the lattice parameter (a_0) of the photocatalyst obtained from the d100 spacing included in Table 1 [29]. The crystallite size of metal in the M-Ti-SBA-15 was calculated according to the Scherrer formula; the results are shown in Table 1. The crystallite size of the photocatalyst was approximately the same value for all types of metal because of pore diameter restrictions.

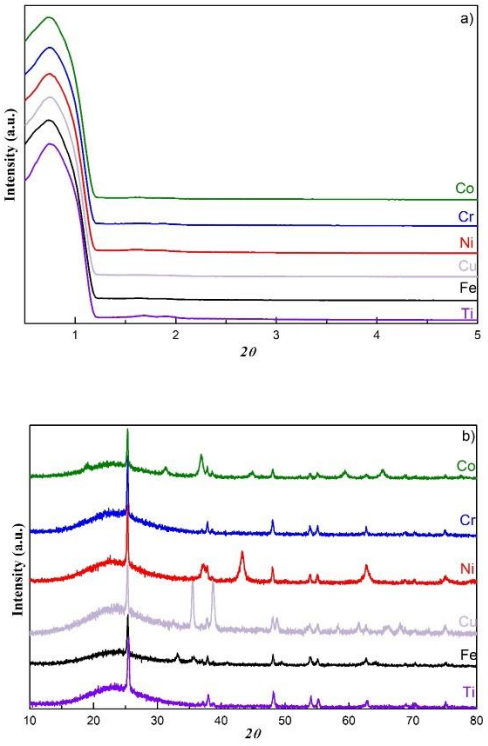

Figure 1. Low-angle XRD patterns (a) and wide-angle XRD patterns (b) of M-Ti-SBA-15 (M=Co, Cr, Ni, Cu, Fe).

Wide-angle XRD patterns of the synthesized catalysts confirm the presence of the crystalline structure of mesoporous M-TiO_2/SBA-15 catalyst (Figure 1b). As shown in Figure 1b, all M-Ti-SBA-15 photocatalysts show a wide and low-intensity peak at $2\theta = 24°$ related to the SBA-15 amorphous walls [17,30,31]. The diffraction peaks obtained from $2\theta \cong 25°$(101), 38° (004), 48° (200), 54° (105), 55° (211), and 63° (204) show the crystal structure of anatase-TiO_2 (JCPDS, 01-084-1285) and the remaining peaks prove the presence of the following metals; Co (JCPDS, 03-065-3103), Cr (JCPDS, 01-073-6548), Ni (JCPDS 65-6920), Cu (JCPDS, 01-080-1916), and Fe (JCPDS, 01-079-5902). A slight deviation after the metal insertion of the anatase TiO_2 peak indexed to the (101) plane at 25.5° indicates that the anatase TiO_2 and the inserted metal are in close contact to promote photogenerated electron transfer and, therefore, photocatalytic efficiency [21].

SEM images of M-Ti-SBA-15 were taken at 15 kV; the results are shown in Figure 2. As shown in

Figure 2a, the SBA-15 has rod-like morphology, which is typical for SBA-15 [32]. In the synthesized photocatalysts, after titania and metal nanoparticles were incorporated into the silica framework, the filamentous structure of SBA-15 remained, which is complies with the small-angle XRD results. Titania particles were distributed evenly on the SBA-15 pore walls in M-Ti-SBA-15 photocatalysts. This phenomenon is also clearly seen in the elemental mapping of Ti in the M-Ti-SBA-15 photocatalyst in Figure 3a. The image of the M-Ti-SBA-15 photocatalyst shows that the metal is well dispersed except for M=Cr, Cu. In these photocatalysts, agglomerated metal particles of different sizes are observed on the external surface of the SBA-15. The elemental mapping images of metals; Co, Cr, Cu, Fe, and Ni show that extremely good distribution was obtained after synthesis, as seen in Figure S1 (Supplementary materials).

The elemental analysis of M-Ti-SBA-15 was determined through XRF analysis and SEM-EDX analyses, as shown in Table 1. The obtained metal loadings in the M-Ti-SBA-15 are in good agreement with the value estimated in the synthesis procedure, except for the Cr metal. The numerical difference between the results of the SEM-EDX and the XRF analyses might have come from analysis techniques; the first is performed on the photocatalyst surface, and the other on the bulk. Only about 2% of the Cr metal was loaded due to the leaching of the Cr during washing in the loading process, as seen in Table 1. In the literature, Cr metal was loaded around 1% at most [33]. The leaching of the Cr might be overcome by loading the Cr metal before the Ti metal.

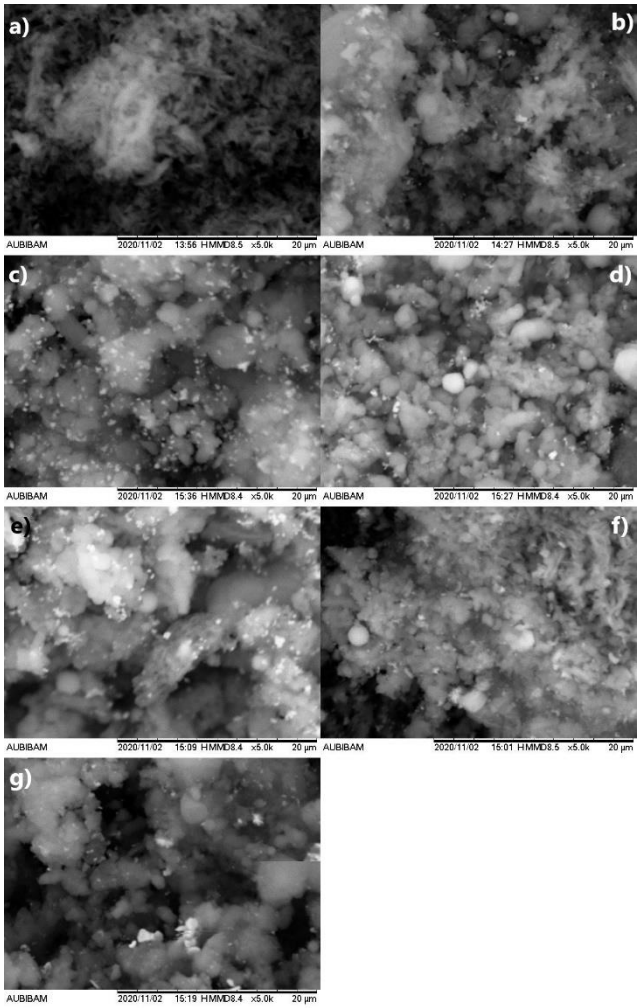

Figure 2. SEM images of SBA-15 (a), Ti-SBA-15 (b), and M-Ti-SBA-15; Co (c), Cr (d), Ni (e), Cu (f), and Fe (g).

Table 1. Structural, chemical, and textural properties of synthesized photocatalysts.

Catalyst	Loading metal amount (%)		Crystallite sizes of TiO_2 (nm)[a]	Surface Area BET[b] (m^2/g)	Pore Volume[c] (cm^3/g)	Pore Diameter (nm)[c]	Lattice parameter a_0(nm)[a]	Pore Wall Thickness nm[d]	Band Gap Energy[e] (eV)[f]
	Determined by XRF	Determined by SEM-EDX							
SBA-15	-	-	-	732	0.89	5.95	13.33	7.38	2.37
Fe-TiO_2/SBA-15	12.8	8.2	10.85	553	0.62	5.40	12.53	7.13	2.04
Cu-TiO_2/SBA-15	7.2	7.5	10.99	460	0.61	5.67	12.69	7.02	3.30
Ni-TiO_2/SBA-15	10.1	7.7	10.92	528	0.67	5.61	12.61	7.00	3.24
Cr-TiO_2/SBA-15	2.5	1.3	10.93	613	0.72	5.55	12.62	7.07	3.24
Co-TiO_2/SBA-15	11.2	7.1	10.87	533	0.62	5.44	12.55	7.11	2.00

[a] From XRD, [b] Multipoint BET method, [c] From BJH method, [d] Wall thickness (a_0 − pore diameter), [e] From UV-DRS

N_2 adsorption-desorption isotherms and the pore size distribution curves of M-Ti-SBA-15 were found using the BJH model from the desorption branch, as shown in Figure 3. According to the IUPAC classification, the synthesized SBA-15 and M-Ti-SBA-15 exhibited type IV characteristic curves with type H1 hysteresis loop [11]. The SBA-15 presents the hysteresis loop at moderate relative pressures ($0.6<p/p_0<0.73$) in a range representing the self-filling of mesopores due to capillary condensation, indicating that maintaining the uniform mesostructure of the SBA-15. All the M-Ti-SBA-15 catalysts also exhibited a similar trend in the hysteresis loop with a slightly higher relative pressure range than the SBA-15. The pore size distribution curves shown in Figure 4b display a uniform pore size of about 7.1 nm with a uniform cylindrical shape for all the samples [30], confirmed by SEM observation.

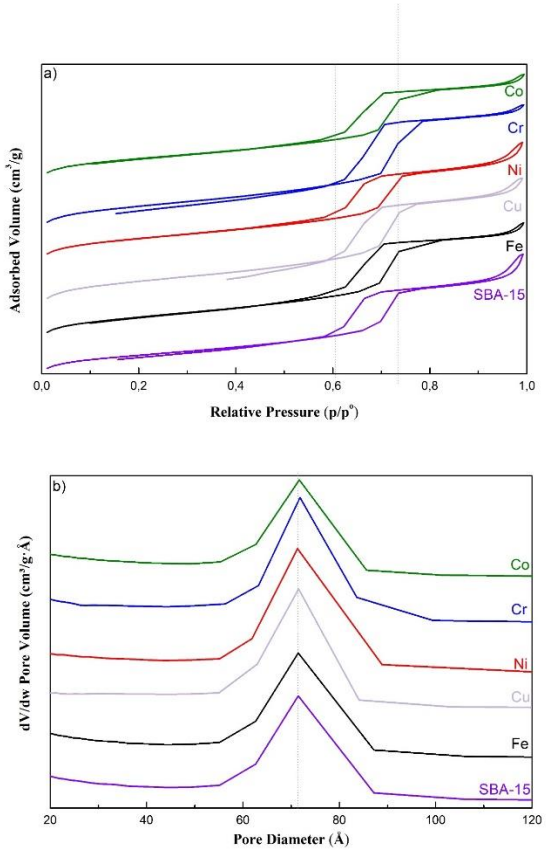

Figure 3. (a) N_2 adsorption-desorption isotherms and (b) pore distributions of M-Ti-SBA-15 (M=Co, Cr, Ni, Cu, Fe).

Textural properties concerning the M-Ti-SBA-15 are presented in Table 1. The decrease in BET surface area, pore volume, pore diameter, and pore wall thickness of the SBA-15 after metal doping perhaps comes from plugging the SBA-15 pores with metal and titania. However, its surface area still falls within the range of high-quality SBA-15, about 500-1000 m^2/g [34]. The textural properties of M-Ti-SBA-15 have minor variations depending on metal types which may be compatible with an ionic radius of metals [35,36]. Meanwhile, the pore wall of M (Fe, Co)-Ti-SBA-15 is thicker than the other metal types considering their ionic radius, which may be attributed to the metal and titania being successfully incorporated inside the mesopore walls [31].

UV-DRS analyses of synthesized photocatalysts are given in Figure 4. It was observed that Ti-SBA-15 has a large absorption drop of around 380 nm, which complies with the absorption on the bandgap of anatase TiO_2 [37]. In addition, the strong adsorption peak at about 350–400 nm demonstrates the TiO_2 particles are larger than 5 nm [38]. After metal doping, the obtained band at 200 nm–240 nm is attributed to the metal-doped SBA-15 framework silica [39]. The absorption range of the synthesized photocatalyst increased compared to the Ti-SBA-15. In particular, the absorption over a broad spectrum range in the Co-Ti-SBA-15 photocatalyst might positively affect the photocatalytic efficiency [40].

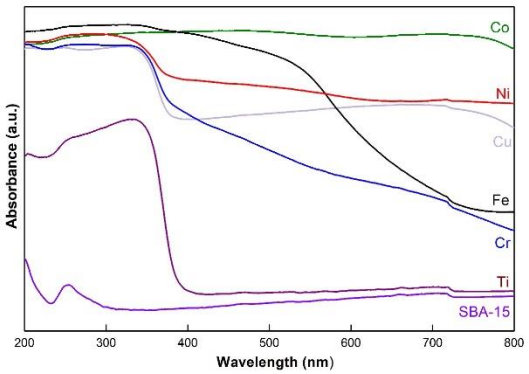

Figure 4. Diffuse reflectance UV-vis spectra of M-Ti-SBA-15 (M=Co, Cr, Ni, Cu, Fe).

The bandgap energy (E_g, eV) was calculated using the Kubelka-Munk function's modified plot, as shown in Figure S2 and Table 1. It is estimated by extrapolation of the linear part of the plot of $[F(R)]\,hv]^2$ versus hv, where h and v are Plank's constant and frequency [14,19].

The calculated values of the optical band gap energies were considerably blue-shift compared with those of the TiO_2 anatase phase (3.2 eV). The decrement in the bandgap energies of photocatalysts indicates quantization effects, which improves the photocatalytic properties.

Photocatalytic properties of M-Ti-SBA-15 and reusability

The photocatalytic activities of M-Ti-SBA-15 were evaluated by the degradation of methylene blue under UV-light irradiation. The results of the photocatalyst

efficiencies are given with adsorption and photocatalyst efficiencies calculated after subtracting the amount of adsorbed dye in Figures 5a and 5b, respectively.

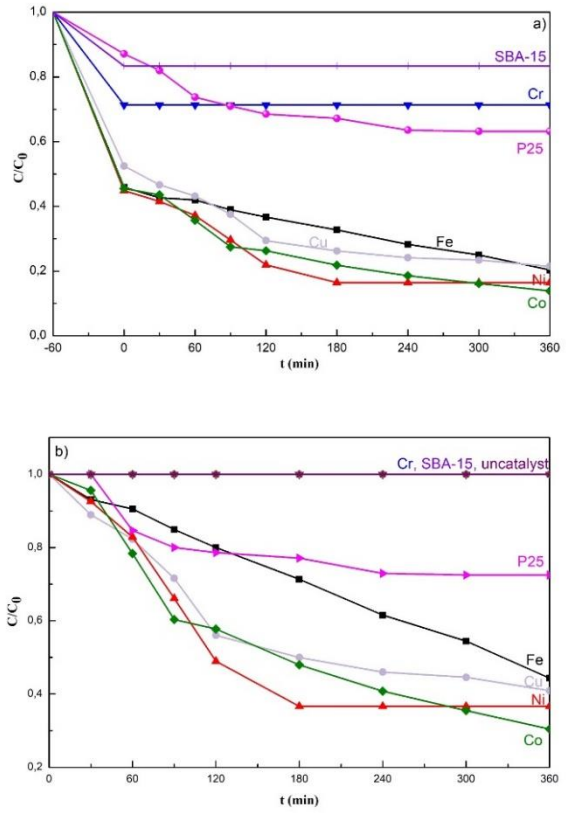

Figure 5. The photocatalytic degradation efficiency of M-Ti-SBA-15 (M=Co, Cr, Ni, Cu, Fe), SBA-15, and Degussa P25 a) with adsorption, and b) with subtracting the adsorption effect (Reaction conditions: 75 m catalyst, 150 mL, 20 mg/L MB aqueous solution).

As shown in Figure 5, no methylene blue degradation was obtained in the absence of catalyst and the presence of pure SBA-15 (Figure 6b). It was observed that only SBA-15 reached the adsorption equilibrium after one hour due to the adsorption properties of the SBA-15 (see Figure 6a). The degradation efficiencies of P25 and M-Ti-SBA-15 (Fe, Cu, Ni, Co) toward MB were 27.6%, 55.7%, 60%, 63.4%, and 69.8% after 360 minutes of irradiation, respectively. The all-metal-doped photocatalyst exhibited higher photoactivity than the Degussa P25 in the conditions where all tested photocatalysts had the same amount of TiO_2, except Cr because little Cr was loaded, as understood from the SEM-EDX and XRF results. This enhanced efficiency could be due to the close contact between the titania and metals, increasing electron mobility to participate in the redox reaction to give active oxygen, which enhances the photodegradation of the methylene blue [2,14,20,41]. In this mechanism, with close contact, the electrons in the metal might be transferred to the conduction band of the TiO_2 and accumulate on the surface (1) of the TiO2 preventing the back transfer of electrons by the Schottky barrier [42]. Transferred electrons might reduce the oxygen on the surface of the Co-Ti-SBA-15 to obtain oxygen radicals ($\cdot O_2$)(2). These radicals might be combined with H_2O to give active species further ($\cdot OH$) (3 and 4). At the same time, the (h^+) ions might be directly oxidized by H_2O. Finally, the produced radicals degrade methylene blue to the products (5). The possible reaction process is as follows:

$$Co-Ti-SBA-15+h\nu \rightarrow Co-Ti-SBA-15\left(e^- + h^+\right) \quad (1)$$

$$Co-Ti-SBA-15\left(e^-\right)+O_2 \rightarrow Co-Ti-SBA-15+\bullet O_2^- \quad (2)$$

$$Co-Ti-SBA-15\left(h^+\right)+H_2O \rightarrow Co-Ti-SBA-15 + \bullet OH + H^+ \quad (3)$$

$$\bullet O_2^- + H^+ \rightarrow \bullet OOH \text{ or } \bullet OH \quad (4)$$

$$Methylene\ blue + \bullet O_2^- + \bullet OH \rightarrow Degradation\ products \quad (5)$$

In addition, the high surface area of the M-Ti-SBA-15 increased the adsorption ability of methylene blue molecules, which directly enhanced the reaction rate [21].

A comparison of the photocatalytic efficiency of Co-Ti-SBA-15 with other SBA-15 nanocomposites is given in Table 2. As can be seen in Table 2, the Co-Ti-SBA-15 is a promising catalyst under the given reaction conditions. Furthermore, in studies comparing the efficiency of the synthesized catalysts with Ti-SBA-15 or Degussa P25 efficiency under the same conditions was examined; Ag-TiO_2/SBA-15 [20] and Au-TiO_2/SBA-15 [21] photocatalysts exhibited 4 and 2 times higher photocatalytic activity than those of TiO_2/SBA-15 and Degussa P25, respectively. Compared with these catalysts, obtaining similar efficiency at the Co-Ti-SBA-15 photocatalyst is promising, making it possible to replace precious elements. Additionally, in another study, the photoactivity of Co-SBA-15 was compared with Degussa P25 under sunlight. The same value was found, which might indicate that enhanced photocatalytic efficiency comes from the synergistic effect of the Co-Ti interaction [43].

Overall, the Co-Ti-SBA-15 photocatalyst showed the highest degradation efficiency; therefore, this sample was selected for evaluation of reusability, as shown in Figure 6. After five cycles, no significant decrease in its photocatalytic activity was observed

Table 2. Comparison of the efficiency of some metal-SBA-15 photocatalysts.

Photocatalyst	Dyes	Reaction Conditions Dye concentration (mg/L)/catalyst dosage (mg) /adsorption time(min)/irradiation source	Catalytic efficiency (%), Time (min)	References
Au/TiO_2/SBA-15	Methylene Blue	20.0/100/30/ visible light (300 W)	100 %, 210	[21]
Ag-TiO_2/SBA-15	Methylene Blue	5.0/100/60/visible light (300 W)	89 %, 30	[20]
Ag/CeO_2/SBA-15	Congo red	0.5/500/30/UV (2.16W) pH = 5.5	100%, 180	[44]
WO_3-SBA-15	Methylene Blue	30/100/-/visible light (500W)	90%, 300	[45]
Fe-Ti-SBA-15	Methylene Blue	15.0/20/60/UV (400W)	82%,180	[46]
TiO_2/SBA-15	Methylene Blue	30.0/20/60/UV (300W)	73 %, 150	[11]
Ag@AgBr/SBA-15	Rhodamine B	20.0/300/60/ UV (500W)	88 %, 300	[47]
Co-SBA-15	Methyl violet	50.0/25/120/Solar radiation pH=6	69 %, 150	[43]
Co-Ti-SBA-15	Methylene Blue	20.0/75/60/ UV (32W)	70%, 360	Present work

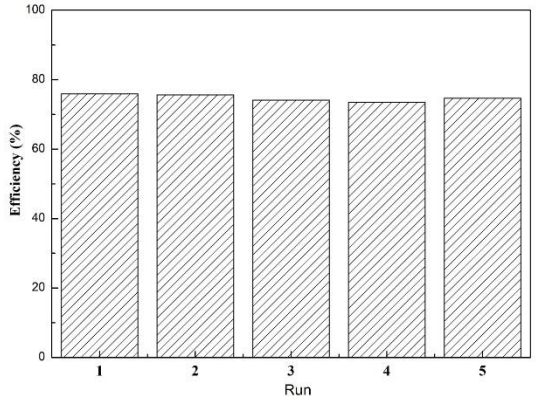

Figure 6. The reusability of Co-Ti-SBA-15.

After this, the reused catalyst was characterized by XRD, SEM-EDX, and N_2 adsorption-desorption isotherms/desorption analyses to determine the structural deviation (Figures S3, S4, and S5 and Table S1). The reused catalyst retained the crystal and hexagonal structure of fresh Co-Ti-SBA-15 and uniform meso structure despite some pore-clogging with the pore size slightly changed from 5.44 nm to 4.76 nm. Furthermore, the obtained metal loadings in the Co-Ti-SBA-15 from the SEM-EDX results were the same as the value of fresh photocatalyst, which showed that no Co-metal leaching occurred during the dye degradation process. Therefore, Co-Ti-SBA-15 maintains its activity and stability after reuse for several cycles.

CONCLUSION

Transition metals (Fe, Cu, Ni, Cr, and Co) were loaded onto highly dispersed TiO_2 within the mesostructured SBA-15. The characterization results show that the expected metal and titania loadings were obtained with a good distribution on SBA-15. Furthermore, the synthesized materials exhibited an intimate contact between the metal and titania, increasing electron mobility and enhancing photocatalytic activity by widening the photo response UV range. Among all the evaluated photocatalysts, Co-Ti-SBA-15 showed a photocatalytic degradation efficiency four times as high as Degussa P25, comparable to the efficiency obtained with precious metals. Therefore, the Co-Ti-SBA-15 photocatalyst, exhibiting excellent reusability of the photocatalytic activity under UV irradiation, may be used in the practical application of pollutant degradation.

ACKNOWLEDGMENT

This study was supported by Eskişehir Technical University Scientific Research Projects Commission under grant no: 22ADP043.

REFERENCES

[1] D.B. Miklos, C. Remy, M. Jekel, K.G. Linden, J.E. Drewes, U. Hübner, Water Res. 139 (2018) 118–131. https://doi.org/10.1016/j.watres.2018.03.042.

[2] D.B. Miklos, C. Remy, M. Jekel, K.G. Linden, J.E. Drewes, U. Hübner, Water Res. 139 (2018) 118–131. https://doi.org/10.1016/j.watres.2018.03.042.

[3] H. Wang, L. Zhang, Z. Chen, J. Hu, S. Li, Z. Wang, J. Liu, X. Wang, Chem. Soc. Rev. 43(15) (2014) 5234–5244. https://doi.org/10.1039/C4CS00126E.

[4] R. Singh S. Dutta, Adv. Powder Technol. 29(2) (2018) 211–219. https://doi.org/10.1016/j.apt.2017.11.005.

[5] M. Saeed, A. Ahmad, R. Boddula, Inamuddin, A.u. Haq, A. Azhar, Environ. Chem. Let 16(1) (2018) 287–294. https://doi.org/10.1007/s10311-017-0661-z.

[6] A. Priya, R.A. Senthil, A. Selvi, P. Arunachalam, C.K. Senthil Kumar, J. Madhavan, R. Boddula, R. Pothu, A.M. Al-Mayouf, Mater. Sci. Energy Technol. 3 (2020) 43–50. https://doi.org/10.1016/j.mset.2019.09.013.

[7] M. Karimi, S. Mansour Bidoki, A. Benvidi, Environ. Eng. Res. 27(3) (2022) 200429–200420. https://doi.org/10.4491/eer.2020.429.

[8] A. Maavia, I. Aslam, M. Tanveer, M. Rizwan, M.W. Iqbal,

M. Tahir, H. Hussain, R. Boddula, M. Yousuf, Mater. Sci. Energy Technol 2(2) (2019) 258–266. https://doi.org/10.1016/j.mset.2019.01.004.

[9] A. Mehta, A. Mishra, M. Sharma, S. Singh, S. Basu, J. Nanopart. Res. 18(7) (2016). https://doi.org/10.1007/s11051-016-3523-x.

[10] A.S.M. Nur, M. Sultana, A. Mondal, S. Islam, F.N. Robel, A. Islam, M.S.A. Sumi, J. Water Process. Eng. 47 (2022) 102728. https://doi.org/10.1016/j.jwpe.2022.102728.

[11] Q. Wei, X.J. Chen, P.F. Wang, Y.B. Han, J.C. Xu, B. Hong, H.X. Jin, D.F. Jin, X.L. Peng, J. Li, Y.T. Yang, H.L. Ge, X.Q. Wang, Chem. Phys. 510 (2018) 47–53. https://doi.org/10.1016/j.chemphys.2018.05.012.

[12] B. Castanheira, L. Otubo, C.L.P. Oliveira, R. Montes, J.B. Quintana, R. Rodil, S. Brochsztain, V.J.P. Vilar, A.C.S.C. Teixeira, Chemosphere 287 (2022) 132023. https://doi.org/10.1016/j.chemosphere.2021.132023.

[13] M.T.P. da Silva, J. Villarroel-Rocha, C.F. Toncón-Leal, F.F. Barbosa, M.O. Miranda, M.A.M. Torres, K. Sapag, S.B.C. Pergher, T.P. Braga, Microporous Mesoporous Mater. 310 (2021). https://doi.org/10.1016/j.micromeso.2020.110582.

[14] L.A. Calzada, R. Castellanos, L.A. García, T.E. Klimova, Microporous Mesoporous Mater. 285 (2019) 247–258. https://doi.org/10.1016/j.micromeso.2019.05.015.

[15] T.-H. Liou, L.-W. Hung, C.-L. Liu, T.-Y. Zhang, J. Porous Mater. 25(5) (2018) 1337–1347. https://doi.org/10.1007/s10934-017-0544-5.

[16] D.S. Conceição, C.A.L. Graça, D.P. Ferreira, A.M. Ferraria, I.M. Fonseca, A.M. Botelho do Rego, A.C.S.C. Teixeira, L.F. Vieira Ferreira, Microporous Mesoporous Mater. 253 (2017) 203–214. https://doi.org/10.1016/j.micromeso.2017.07.013.

[17] M.M. Araújo, L.K.R. Silva, J.C. Sczancoski, M.O. Orlandi, E. Longo, A.G.D. Santos, J.L.S. Sá, R.S. Santos, G.E. Luz, L.S. Cavalcante, Appl. Surf. Sci. 389 (2016) 1137–1147. https://doi.org/10.1016/j.apsusc.2016.08.018.

[18] G. Li, B. Wang, W.Q. Xu, Y. Han, Q. Sun, Dyes Pigm. 155 (2018) 265–275. https://doi.org/10.1016/j.dyepig.2018.03.058.

[19] M. Filip, G. Petcu, E.M. Anghel, S. Petrescu, B. Trica, P. Osiceanu, N. Stanica, I. Atkinson, C. Munteanu, M. Mureseanu, V. Parvulescu, Catal. Today 366 (2021) 10–19. https://doi.org/10.1016/j.cattod.2020.08.003.

[20] L. Liang, Y. Meng, L. Shi, J. Ma, J. Sun, Superlattices Microstruct. 73 (2014) 60–70. https://doi.org/10.1016/j.spmi.2014.05.008.

[21] Y. Chen, J. Wang, W. Li, M. Ju, Mater. Lett. 159 (2015) 131–134. https://doi.org/10.1016/j.matlet.2015.04.030.

[22] F. Chang, J. Wang, J. Luo, J. Sun, B. Deng, X. Hu, Colloids Surf. A. Physicochem. Eng. Asp. 499 (2016) 69–78. https://doi.org/10.1016/j.colsurfa.2016.04.013.

[23] T.T. Nguyen, E.W. Qian, Microporous Mesoporous Mater. 265 (2018) 1–7. https://doi.org/10.1016/j.micromeso.2018.01.026.

[24] D.C. Khandekar, A.R. Bhattacharyya, R. Bandyopadhyaya, J. Environ. Chem. Eng. 7(5) (2019) 103433. https://doi.org/10.1016/j.jece.2019.103433.

[25] Y. Soni, S. Gupta, C.P. Vinod, Mol. Catal. 511 (2021). https://doi.org/10.1016/j.mcat.2021.111732.

[26] W. Gao, X. Tang, H. Yi, S. Jiang, Q. Yu, X. Xie, R. Zhuang, J. Environ. Sci. 125 (2023) 112–134. https://doi.org/10.1016/j.jes.2021.11.014.

[27] E. Akbay, T.G. Ölmez, Mater. Lett. 215 (2018) 263–267. https://doi.org/10.1016/j.matlet.2017.12.117.

[28] K. Chandra Mouli, S. Mohanty, Y. Hu, A. Dalai, J. Adjaye, Catal. Today 207 (2013) 133–144. https://doi.org/10.1016/j.cattod.2012.07.010.

[29] I.C. Nogueira, L.S. Cavalcante, P.F.S. Pereira, M.M. De Jesus, J.M. Rivas Mercury, N.C. Batista, M.S. Li, E. Longo, J. Appl. Crystallogr. 46(5) (2013) 1434–1446. https://doi.org/10.1107/S0021889813020335.

[30] T. Qiang, Y. Song, J. Zhao, J. Li, J. Alloys Compd. 770 (2019) 792–802. https://doi.org/10.1016/j.jallcom.2018.08.074.

[31] R. Malik, P.S. Rana, V.K. Tomer, V. Chaudhary, S.P. Nehra, S. Duhan, Microporous Mesoporous Mater. 225 (2016) 245–254. https://doi.org/10.1016/j.micromeso.2015.12.013.

[32] P. Tamizhdurai, S. Narayanan, R. Kumaran, V.L. Mangesh, C. Kavitha, N. Vidhya Lakshmi, C. Ragupathi, Z.A. Alothman, M. Ouladsmane, G. Mani, Adv. Powder Technol. 32(11) (2021) 4286–4294. https://doi.org/10.1016/j.apt.2021.09.033.

[33] V.R. Elías, G.O. Ferrero, R.G. Oliveira, G.A. Eimer, Microporous Mesoporous Mater. 236 (2016) 218–227. https://doi.org/10.1016/j.micromeso.2016.09.001.

[34] W. Zhan, J. Yao, Z. Xiao, Y. Guo, Y. Wang, Y. Guo, G. Lu, Microporous Mesoporous Mater. 183 (2014) 150–155. https://doi.org/10.1016/j.micromeso.2013.08.038.

[35] S.B.A. Hamid, N.A. Daud, D.D. Suppiah, W.A. Yehya, P. Sudarsanam, S.K. Bhargava, Polyhedron 120 (2016) 154–161. https://doi.org/10.1016/j.poly.2016.08.027.

[36] M.J. da Silva, L.C. de Andrade Leles, M.G. Teixeira, React. Kinet.Mech.Catal. 131(2) (2020) 875–887. https://doi.org/10.1007/s11144-020-01888-4.

[37] A. Wróblewska, P. Miądlicki, J. Sreńscek-Nazzal, M. Sadłowski, Z.C. Koren, B. Michalkiewicz, Microporous Mesoporous Mater. 258 (2018) 72–82. https://doi.org/10.1016/j.micromeso.2017.09.007.

[38] Y.J. Acosta-Silva, R. Nava, V. Hernández-Morales, S.A. Macías-Sánchez, M.L. Gómez-Herrera, B. Pawelec, Appl. Catal., B. 110 (2011) 108–117. https://doi.org/10.1016/j.apcatb.2011.08.032.

[39] R. Pothu, H. Mitta, R. Boddula, P. Balla, R. Gundeboyina, V. Perugopu, J. Ma, Mater. Sci. Technol. 5 (2022) 391–398. https://doi.org/10.1016/j.mset.2022.09.006.

[40] P.V. Suraja, Z. Yaakob, N.N. Binitha, M.R. Resmi, P.P. Silija, Chem. Eng. J. 176-177 (2011) 265–271. https://doi.org/10.1016/j.cej.2011.05.071.

[41] M.K. Sahu, R.K. Patel, J. Ind. Eng. Chem. 40 (2016) 72–82. https://doi.org/10.1016/j.jiec.2016.06.008.

[42] J.S. DuChene, B.C. Sweeny, A.C. Johnston-Peck, D. Su, E.A. Stach, W.D. Wei, Angew. Chem. Int. Ed. 53(30) (2014) 7887–7891. https://doi.org/10.1002/anie.201404259.

[43] F. Xia, E. Ou, L. Wang, J. Wang, Dyes Pigm. 76(1) (2008) 76–81. https://doi.org/10.1016/j.dyepig.2006.08.008.

[44] L.F. Chen, U. Arellano, J.A. Wang, L.M. Balcázar, R. Sotelo, S. Solis, M. Azomosa, J. González, O.A. González Vargas, Y. Song, J. Liu, X.L. Zhou, Catal. Today 394–396 (2022) 62-80. https://doi.org/10.1016/j.cattod.2021.10.014.

[45] S. Kumaravel, S. Thiripuranthagan, T. Vembuli, E. Erusappan, M. Durai, T. Sureshkumar, M. Durai, Optik 235 (2021) 166599. https://doi.org/10.1016/j.ijleo.2021.166599.

[46] F. Chang, M. Jiao, Q. Xu, B. Deng, and X. Hu, Appl. Surf. Sci. 435 (2018) 708–717. https://doi.org/10.1016/j.apsusc.2017.11.168.

[47] L. Hu, H. Yuan, L. Zou, F. Chen, X. Hu, Appl. Surf. Sci. 355 (2015) 706–715. https://doi.org/10.1016/j.apsusc.2015.04.166.

SEVGI CAN GÖL
ELIF AKBAY

Eskişehir Technical University,
Dept. of Chemical Engineering,
İki Eylül Campus, Eskişehir,
Turkey

NAUČNI RAD

EFEKAT INTERAKCIJE METAL-TITANIUM NA FOTODEGRADACIJU U FOTOKATALIZATORIMA METAL-TITANIUM NANETIM NA SBA-15

Nekoliko prelaznih metala (Fe, Cu, Ni, Cr i Co) je ubačeno u Ti-SBA-15 korišćenjem metoda sinteze u dva koraka. Za karakterizaciju su korišćene analize XRD, SEM-EDX, izoterme adsorpcije-desorpcije N_2, XRF i UV-DRS. Rezultati su potvrdili očuvanje uređene mezoporozne strukture, dobro dispergovanog Ti-metala i poboljšanu apsorpciju svetlosti u poređenju sa Ti-SBA-15. Fotokatalitičke performanse su procenjene u degradaciji metilenskog plavog pod UV svetlom. Rezultati pokazuju da je Co-Ti-SBA-15 pokazao najveću fotokatalitičku aktivnost među pripremljenim fotokatalizatorima za razgradnju metilenskog plavog. Značajno povećanje aktivnosti može se pripisati povećanoj adsorpciji reaktanata mezoporoznom strukturom SBA-15, dobroj distribuciji TiO_2 u porama SBA-15 i povećanoj pokretljivosti prenosa elektrona usled dopinga metala. Pored efikasnosti, Co-Ti-SBA-15 je pogodan katalizator za degradaciju boje, pokazujući dobru stabilnost u degradaciji metilen plavog tokom pet fotokatalitičkih ciklusa bez ikakvog odstupanja strukture.

Ključne reči: prelazni metali, mezoporozni materijal, Ti-SBA-15, fotokatalitička degradacija, ponovna upotreba.